Evaluation of field-induced magnetic moments in the spin-$\frac{1}{2}$ antiferromagnetic trimerized chain compound $Cu_3(P_2O_6OD)_2$

Masashi Hase,[1,*] Vladimir Yu. Pomjakushin,[2] Lukas Keller,[2] Uwe Stuhr,[2]
Andreas Dönni,[3] Masanori Kohno,[3] and Akihiro Tanaka[3]

[1]*Research Center for Advanced Measurement and Characterization, National Institute for Materials Science (NIMS), 1-2-1 Sengen, Tsukuba, Ibaraki 305-0047, Japan*

[2]*Laboratory for Neutron Scattering and Imaging, Paul Scherrer Institut (PSI), CH-5232 Villigen PSI, Switzerland*

[3]*International Center for Materials Nanoarchitectonics (WPI-MANA), National Institute for Materials Science (NIMS), 1-1 Namiki, Tsukuba, Ibaraki 305-0044, Japan*

(Received 9 December 2019; revised 17 June 2020; accepted 18 June 2020; published 6 July 2020)

We report on our evaluation of field-induced magnetic moments in the paramagnetic state of the spin-$\frac{1}{2}$ antiferromagnetic trimerized ($J_1 - J_2 - J_2$) chain compound $Cu_3(P_2O_6OD)_2$ with $J_1 = 111$ K and $J_2 = 30$ K [M. Hase *et al.*, Phys. Rev. B **76**, 064431 (2007)]. Magnetic reflections with integer indices, generated by field-induced magnetic moments, were observed at neutron-diffraction experiments performed in an applied magnetic field, and we evaluated the magnitudes of the moments to be $M_1 = 0.43(2)\,\mu_B$/Cu and $M_2 = 0.013(10)\,\mu_B$/Cu on the two crystallographic Cu^{2+} (Cu1 and Cu2) sites, respectively, at 6 T and 1.6 K. The resulting ratio $M_2/M_1 = 0.03(2)$ is in good agreement with the theoretical value for the ratio of the magnetization at the two sites. We thus conclude that for this well-understood spin system (which has the advantage of being amenable to detailed theoretical calculations) the extracted field-induced magnetic moments reproduce the correct information on the magnetization. Our result leads us to believe that we can precisely evaluate exchange interactions in paramagnets with multiple exchange interactions and multiple crystallographic magnetic-ion sites by using field-induced magnetic moments in combination with macroscopic physical quantities. This idea is expected to be applicable to a wide variety of quantum and frustrated magnets without long-range order.

DOI: 10.1103/PhysRevB.102.014403

I. INTRODUCTION

The precise knowledge on exchange interactions is clearly a prerequisite toward understanding the magnetic properties of quantum spin systems. Exchange interactions are often evaluated using macroscopic physical quantities such as magnetization and specific heat. There are cases, however, in which the use of such measurements alone can lead to ambiguity, where the results of experiments are seemingly accountable by several alternative sets of exchange interactions, as is seen in the spin-$\frac{1}{2}$ diamond chain compound $Cu_3(CO_3)_2(OH)_2$ (azurite) [1–5].

We can evaluate exchange interactions in a more precise manner by combing neutron-scattering results and macroscopic physical quantities. Exchange interactions can be reliably determined through the dispersion relations of magnetic excitations that are observed in inelastic neutron-scattering (INS) experiments, especially after having gained knowledge from the macroscopic physical quantities and the crystal structure as to which exchange interactions are likely to be dominant. A major setback of this scheme, however, is that INS experiments usually require the use of large single crystals, limiting its availability. Inputs from neutron-diffraction experiments on ordered magnetic moments are also useful, as they can be used to clarify the signs of the exchange interactions and the ratios among the exchange-interaction values. This approach was applied, e.g., to the spin tetramer (four-spin system) compounds $Cu_2Fe_2Ge_4O_{13}$ [6,7] and $Cu_2CdB_2O_6$ [8]. The powerfulness of this strategy may be highlighted in particular through its application to the latter compound, where it enabled the authors to correct a previous assignment [9] of a wrong sign to one of the exchange constants, resulting in a totally new (and correct) set of exchange interactions [8]. The method, however, is apparently inapplicable to paramagnets as they have no ordered magnetic moments.

In a similar vein, it would seem natural to expect that the *field-induced* magnetic moments determined using neutron-diffraction experiments in magnetic fields should be useful for evaluating the exchange interactions of *paramagnets*. Let us take, for example, the trimerized ($J_1 - J_2 - J_2$) spin chain depicted in Fig. 1 and consider its response to a magnetic field. First consider the case where the antiferromagnetic (AFM) J_1 interaction is dominant. The Cu2 spins will in this case pair up into AFM dimers. Upon applying a magnetic field, the field-induced magnetic moments on both the Cu1 and Cu2 sites will align parallel to the magnetic fields, as also illustrated in Fig. 1. In weak magnetic fields, the magnitude of the moment on Cu1 sites is greater than that on Cu2 sites. On the other hand, if the AFM J_2 interaction is dominant, AFM trimers

*HASE.Masashi@nims.go.jp

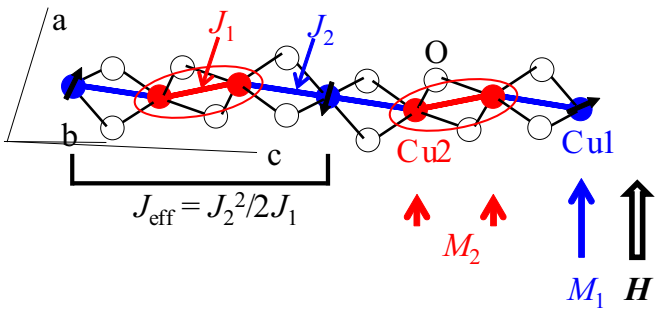

FIG. 1. Spin system and expected field-induced magnetic moments in $Cu_3(P_2O_6OD)_2$ [10,11]. Cu^{2+} ions ($3d^9$) have a localized spin ($S = \frac{1}{2}$). Two crystallographic Cu (Cu1 and Cu2) sites exist [12]. The red and blue bars represent the shortest and second-shortest Cu-Cu pairs, whose Cu-Cu lengths are 3.06 Å and 3.28 Å at room temperature, respectively. The other Cu-Cu lengths are 4.27 Å or longer. The J_1 and J_2 exchange interactions in the shortest and second-shortest Cu-Cu pairs, respectively, form a spin-$\frac{1}{2}$ trimerized $(J_1 - J_2 - J_2)$ chain whose Hamiltonian is expressed as follows: $\mathcal{H} = \sum_i J_1 S_i S_{i+1} + J_2 S_{i+1} S_{i+2} + J_2 S_{i+2} S_{i+3}$. The J_1 and J_2 interactions were evaluated to be 111 and 30 K, respectively [11]. The red ellipse denotes a spin-singlet-like pair at an AFM dimer. The spins (black arrows) on the Cu1 sites are coupled to one another by the $J_{\rm eff}$ interaction ($J_{\rm eff} = \frac{J_2^2}{2J_1} = 4.1$ K). The arrows at the bottom depict the field-induced magnetic moments, M_1 and M_2, on the Cu1 and Cu2 sites, respectively.

(three-spin systems) are formed. In weak magnetic fields, the field-induced magnetic moments on Cu1 and Cu2 sites are antiparallel and parallel to the magnetic fields, respectively.

There are several previous reports on the evaluation of field-induced magnetic moments in paramagnets. Paschen *et al.* showed that the Ce moments at the 4a site were smaller by at least a factor of 2 than those at the 8c sites in paramagnetic $Ce_3Pd_{20}Si_6$ [13]. In the spin-$\frac{5}{2}$ AFM trimer compound $SrMn_3P_4O_{14}$ [14], we evaluated the field-induced magnetic moments at 6 T and 1.6 K, where a $\frac{1}{3}$ quantum magnetization plateau appeared [15]. The magnetization plateau indicated that the ground state (GS) was a sort of fully polarized paramagnetic state. The Hamiltonian of a spin trimer is expressed as follows: $\mathcal{H} = J(S_1 S_2 + S_2 S_3)$. In the plateau GS, the quantum-mechanical values were calculated to be $S_{1z} = S_{3z} = \frac{15}{7}$ and $S_{2z} = -\frac{25}{14}$. We confirmed that the experimentally evaluated field-induced magnetic moment on each site was the same as gS_{jz}, where g denoted the g factor.

To demonstrate that the exchange interactions can be precisely evaluated in paramagnets by using field-induced magnetic moments in combination with macroscopic physical quantities such as magnetization and specific heat, it is necessary to confirm whether the experimental values of field-induced magnetic moments are consistent with the calculated ones of magnetizations in well-understood spin systems. To this end we focus in this study on $Cu_3(P_2O_6OD)_2$. No signature of magnetic long-range order (LRO) appears down to 2 K in the specific-heat result [10]. As detailed in Fig. 1, the spin degrees of freedom of this material form a spin-$\frac{1}{2}$ AFM trimerized $(J_1 - J_2 - J_2)$ chain. The AFM exchange interactions were evaluated to be $J_1 = 111$ K and $J_2 = 30$ K [11]. The spins on the Cu2 sites are coupled by the most dominant J_1 interaction and form AFM spin dimers. The spins on the neighboring Cu1 sites in a chain are weakly and antiferromagnetically coupled to one another through the intermediate AFM spin dimer and form an AFM spin chain whose effective interaction ($J_{\rm eff}$) is expressed as $\frac{J_2^2}{2J_1}$. Therefore the magnetizations on the Cu2 and Cu1 sites are small and large, respectively. The calculated magnetizations are shown in Fig. 4(b) of Ref. [10]. The magnetization of Cu2 is approximately zero in weak magnetic fields, whereas that of Cu1 appears even in significantly weak magnetic fields. As we now describe in detail, we performed neutron-diffraction experiments on $Cu_3(P_2O_6OD)_2$ polycrystalline pellets, experimentally evaluated the field-induced magnetic moments (M_1 and M_2 on the Cu1 and Cu2 sites, respectively), and compared the values with the calculated magnetizations on the Cu sites.

II. METHODS OF EXPERIMENTS AND CALCULATION

We synthesized a crystalline powder of $Cu_3(P_2O_6OD)_2$ from a mixture of CuO (5 g) and D_3PO_4-D_2O (200 mL) [12]. The mixture was stirred continuously while heating it until the CuO was completely dissolved. Subsequently, the mixture was placed in a furnace in air at 463 K for 48 h. Consequently, $Cu_3(P_2O_6OD)_2$ appeared as a light blue powder. We measured the x-ray powder diffraction pattern at room temperature (T) using a diffractometer (Rigaku RINT-TTR III). Most reflections originated from $Cu_3(P_2O_6OD)_2$. In addition, we detected significantly weak reflections of other materials.

We performed neutron-diffraction experiments at the Swiss spallation neutron source (SINQ) in the Paul Scherrer Institut (PSI), where we used the high-resolution powder diffractometer for thermal neutrons (HRPT) [16] and the high-intensity cold neutron powder diffractometer (DMC). The wavelengths of the neutrons were $\lambda = 1.89$ and 4.51 Å for the HRPT and DMC experiments, respectively. We applied magnetic fields in the range of $\mu_0 H = 0$–6 T almost perpendicularly to the scattering vectors ($\mathbf{Q}$) by using a superconducting magnet. We used pressed polycrystalline pellets of $Cu_3(P_2O_6OD)_2$ with a diameter of 8 mm to minimize the problem of powder realignment in the presence of strong magnetic fields.

We performed the Rietveld refinements of the crystal structure using the FULLPROF SUITE program package [17]. We describe the calculation method for the integrated intensities of the magnetic reflections generated by the field-induced magnetic moments in Sec. III.

We calculated the magnetic-field dependence of the magnetization of the spin-$\frac{1}{2}$ AFM trimerized chain by quantum Monte Carlo (QMC) techniques using the directed-loop algorithm in the path-integral formulation [18]. The number of Cu sites in the QMC simulations was 120. We performed more than one million updates.

III. RESULTS AND DISCUSSION

The circles in Fig. 2(a) depict the neutron-diffraction pattern of $Cu_3(P_2O_6OD)_2$ pellets at 0 T and 1.8 K measured using the HRPT diffractometer. The wavelength of the neutrons (λ) was 1.89 Å. We performed Rietveld refinements using $P\bar{1}$ (no. 2) to evaluate the crystal-structure parameters. The line on the

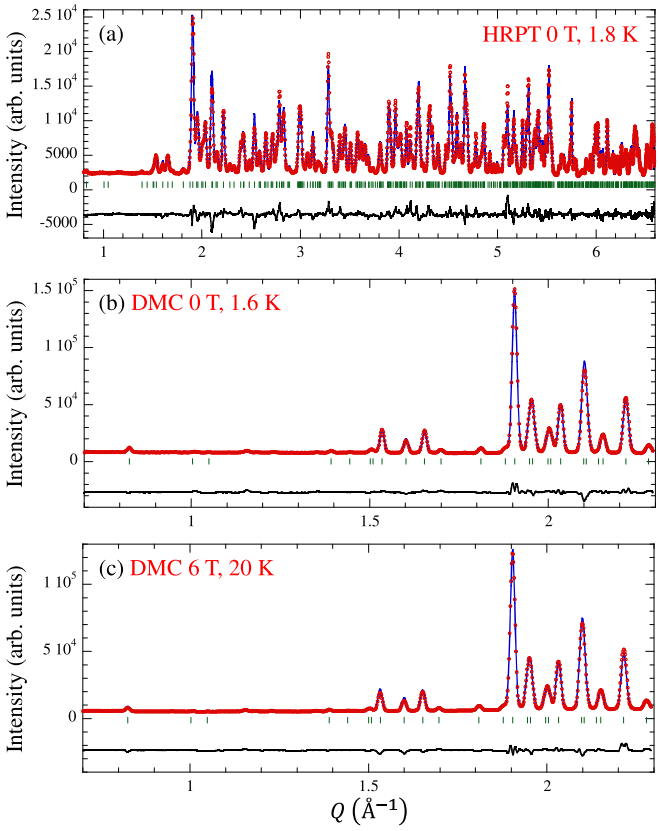

FIG. 2. Neutron-diffraction patterns (circles) of $Cu_3(P_2O_6OD)_2$ polycrystalline pellets (a) measured using the HRPT diffractometer ($\lambda = 1.89$ Å) at 0 T and 1.8 K and measured using the DMC diffractometer (4.51 Å) at (b) 0 T and 1.6 K, and (c) 6 T and 20 K. The line on the measured pattern portrays the Rietveld-refined pattern obtained using the crystal structure with $P\bar{1}$ (no. 2). The line at the bottom portrays the difference between the measured and Rietveld-refined patterns. The hash marks represent the positions of nuclear reflections.

experimental pattern indicates the result of the refinements. The line is in good agreement with the experimental pattern. The values of the crystal-structure parameters presented in Table I are consistent with those obtained in the previous refinements of an x-ray diffraction pattern [12]. Therefore we consider that no alignment of the powder occurs during the production of the pellets. In this study, we could determine the deuterium position.

The circles in Figs. 2(b) and 2(c) depict the neutron-diffraction patterns of $Cu_3(P_2O_6OD)_2$ pellets at 0 T and 1.6 K and at 6 T and 20 K, respectively, measured using the DMC diffractometer ($\lambda = 4.51$ Å). We performed Rietveld refinements using the values of the crystal-structure parameters presented in Table I. The results of the refinements are also shown in Figs. 2(b) and 2(c). The refined pattern is in good agreement with the experimental one in each figure. Consequently, we could not detect the magnetic reflections at either 0 T and 1.6 K or at 6 T and 20 K within experimental accuracy. The agreement between the refined and experimental patterns in Fig. 2(c) indicates that no alignment of the powder in the pellets occurred upon the application of magnetic fields.

TABLE I. Values of crystal-structural parameters of $Cu_3(P_2O_6OD)_2$ derived from the Rietveld refinements of the HRPT neutron powder diffraction pattern at 0 T and 1.8 K. The term B_{iso} denotes the isotropic atomic displacement parameter. We used monoclinic $P\bar{1}$ (no. 2). The lattice constants are $a = 4.7735(1)$ Å, $b = 7.0365(2)$ Å, $c = 8.3315(2)$ Å, $\alpha = 66.570(1)^\circ$, $\beta = 77.063(1)^\circ$, and $\gamma = 72.001(1)^\circ$. The estimated standard deviations are shown in the parentheses. The reliability indices of the refinements are $R_p = 4.74\%$, $R_{wp} = 6.07\%$, $R_{exp} = 1.02\%$, and $\chi^2 = 35.7$.

Atom	Site	x	y	z	B_{iso} Å^2
Cu1	1a	0	0	0	0.07(4)
Cu2	2i	0.9389(6)	0.8461(4)	0.4291(4)	0.07(4)
P1	2i	0.6339(9)	0.5084(7)	0.7072(6)	0.52(6)
P2	2i	0.6498(9)	0.8405(7)	0.8133(6)	0.52(6)
O1	2i	0.6842(9)	0.6617(6)	0.5177(4)	0.23(3)
O2	2i	0.8186(9)	0.9445(6)	0.6332(4)	0.23(3)
O3	2i	0.2930(8)	0.5142(6)	0.7427(5)	0.23(3)
O4	2i	0.6921(8)	0.6003(5)	0.8364(5)	0.23(3)
O5	2i	0.7779(9)	0.8280(6)	0.9679(5)	0.23(3)
O6	2i	0.1759(8)	0.7199(6)	0.2529(4)	0.23(3)
O7	2i	0.3171(8)	0.9452(6)	0.8119(5)	0.23(3)
D1	2i	0.2499(9)	0.3899(6)	0.8460(5)	1.94(9)

The circles in Fig. 3(a) depict the difference pattern at 6 T obtained by subtracting the pattern at 20 K from that at 1.6 K. We can see several reflections that are not artifacts from the subtraction of the data because of the following findings. The diffraction pattern at 6 T and 20 K is depicted in Fig. 3(b). We can see the reflections of other materials between

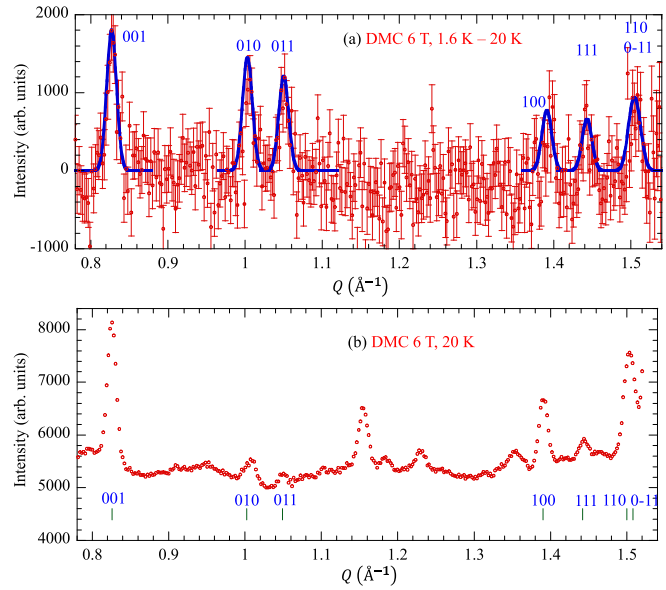

FIG. 3. (a) Difference pattern at 6 T obtained by subtracting the pattern at 20 K from that at 1.6 K. We labeled the indices of several magnetic reflections generated by field-induced magnetic moments. The blue lines show the calculated reflections. (b) The neutron-diffraction pattern at 6 T and 20 K. It is a magnified version of that in Fig. 2(c). The hash marks represent the positions of the nuclear reflections of $Cu_3(P_2O_6OD)_2$.

$Q = 1.14$ and 1.37 Å^{-1}. However, the reflections are not seen in Fig. 3(a), indicating that the subtraction was appropriately performed. In Fig. 3(a), the reflections at 001, 010, and 011 are clearly prominent. The intensity of the 001 reflection is highest, and those of the 010 and 011 reflections are approximately equal to each other. In addition, the reflections at 100, 111, 110, and 0−11 may exist.

We deduce that the reflections are generated by field-induced magnetic moments because of the following findings. The magnetic susceptibility is finite at low T [10]. No magnetic LRO, however, appears in weak magnetic fields at low T, indicating that the system can be effectively regarded as almost decoupled spin chains, as depicted in Fig. 1. Therefore, a magnetic LRO dose not occur at 6 T and low T, and it cannot be the origin of the reflections.

We calculated the integrated intensities $[I_{\rm M}(\mathbf{Q})]$ of the magnetic reflections generated by field-induced magnetic moments as follows:

$$I_{\rm M}(\mathbf{Q}) = A|F_{\rm M}(\mathbf{Q})|^2 n_{\mathbf{Q}} \frac{1}{\sin 2\theta \sin\theta}, \tag{1}$$

where

$$F_{\rm M}(\mathbf{Q}) = -\frac{1}{2}\frac{\gamma e^2}{m_e c^2}\sum_j f(Q)_j m_j \exp(i\mathbf{Q}\cdot\mathbf{r}_j) \times \exp\left(-B_j\frac{\sin^2\theta}{\lambda^2}\right). \tag{2}$$

The coefficient A in Eq. (1) denotes a scaling factor that is common to the magnetic and nuclear reflections. We evaluated A to be 1.008×10^{28} cm^{-2} using the Rietveld refinements for the crystal structure at 6 T and 20 K depicted in Fig. 2(c). The term $n_{\mathbf{Q}}$ denotes the number of reflections with the same intensity and $|\mathbf{Q}|$. The term 2θ denotes the scattering angle. The value of $\frac{\gamma e^2}{m_e c^2}$ is 5.39×10^{-13} cm. The summation in Eq. (2) is performed within the unit cell. The terms $\mathbf{r}_j$, $f(Q)_j$, m_j, and B_j denote the position of the jth site ion, magnetic form factor [19], field-induced magnetic moment, and atomic displacement parameter, respectively. We used the atomic positions and values of B_j listed in Table I.

Here we explain the reason for our use of the scalar m_j instead of the vector $\mathbf{m}_{j\perp\mathbf{Q}}$, where $\mathbf{m}$ and $\mathbf{m}_{j\perp\mathbf{Q}}$ denote the magnetic-moment vector and the perpendicular component of $\mathbf{m}$ to $\mathbf{Q}$, respectively. Because the perpendicular components contribute to the magnetic reflections, $\mathbf{m}_{j\perp\mathbf{Q}}$ is used to calculate the magnetic reflections generated by the magnetic LRO. In this study we applied the magnetic fields almost perpendicular to $\mathbf{Q}$. The field-induced magnetic moments are always almost perpendicular to $\mathbf{Q}$. Therefore we input the scalar m_j in Eq. (2).

The calculated intensity ratio of the magnetic reflections is depicted in Fig. 4. The intensity ratios strongly depend on M_2/M_1. From the experimental value of $I(001)/I(010) = 1.24(14)$, indicated by the horizontal line, we determined M_2/M_1 to be 0.03(2). The blue lines in Fig. 3(a) depict the magnetic reflections calculated for $M_1 = 0.43\,\mu_{\rm B}$/Cu and $M_2 = 0.013\ \mu_{\rm B}$/Cu ($M_2/M_1 = 0.03$), and they can explain the experimental results. The calculated intensity ratio $I(011)/I(010)$, indicated using the squares in Fig. 4, decreases

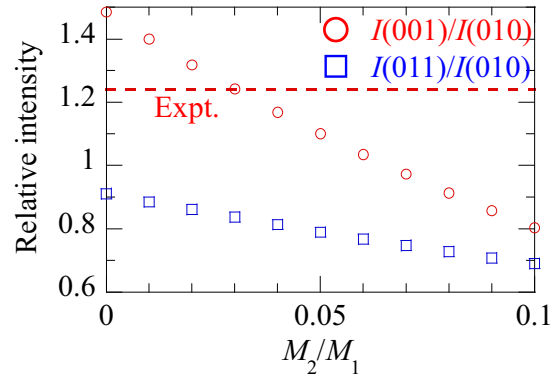

FIG. 4. Calculated intensity ratio of the magnetic reflections vs M_2/M_1. The horizontal line indicates the experimental value of $I(001)/I(010) = 1.24$.

with increasing M_2/M_1, thereby indicating that the M_2/M_1 value of 0.05 or more cannot explain the experimental intensity ratio of $I(011)/I(010)$. We estimated the error bars of M_1 and M_2 to be $0.02\,\mu_{\rm B}$/Cu and $0.01\,\mu_{\rm B}$/Cu, respectively, by using the error bar of M_2/M_1 (0.02). As expected for $Cu_3(P_2O_6OD)_2$, the field-induced magnetic moments on the Cu1 and Cu2 sites are large and small, respectively.

We calculated the magnetizations of Cu1 and Cu2 to be $0.525\,\mu_{\rm B}$/Cu and $0.016\,\mu_{\rm B}$/Cu, respectively, in the spin-$\frac{1}{2}$ AFM trimerized chain with $J_1 = 111$ K and $J_2 = 30$ K at 6 T and 1.6 K by using the QMC techniques. The ratio between both the magnetizations is 0.03 and is consistent with M_2/M_1. The value of M_1 [$0.43(2)\,\mu_{\rm B}$/Cu], however, is smaller than that of the magnetization of Cu1 ($0.525\,\mu_{\rm B}$/Cu). We consider the reason for the difference in the following. Similar results were obtained in $SrMn_3P_4O_{14}$ [15]. As previously described, the field-induced magnetic moment on each Mn site evaluated in the experiments is the same as the corresponding calculated magnetization at 6 T and 1.6 K, where the $\frac{1}{3}$ quantum magnetization plateau appears. As depicted in Fig. 4(c) in [15], on the other hand, the normalized intensity of the magnetic reflection at 011 generated by the field-induced magnetic moments is smaller than the square of the magnetization above 7 K, thereby indicating that the magnetization comprises the field-induced magnetic moments and fluctuating components. In $Cu_3(P_2O_6OD)_2$, the magnetization increases with increasing $\mu_0 H$ at 6 T and 1.6 K and therefore comprises the field-induced magnetic moments and fluctuating components. Accordingly, the value of M_1 is smaller than that of the magnetization of Cu1. A $\frac{1}{3}$ quantum magnetization plateau appears in the magnetic fields of $\mu_0 H > 12$ T at 1.6 K in $Cu_3(P_2O_6OD)_2$. We expect the value of the field-induced magnetic moment on each site to be the same as that of the calculated magnetization on the corresponding site in the plateau magnetic fields, as in $SrMn_3P_4O_{14}$ [15].

Let us now mention some noteworthy characteristics of our method. We could evaluate significantly small M_2, although the error bar was considerable. As previously described, in the case wherein the magnetic fields are applied perpendicularly to $\mathbf{Q}$, the field-induced magnetic moments are also perpendicular to $\mathbf{Q}$. Because the magnetic moments perpendicular to

Q contribute to the magnetic reflections, small field-induced magnetic moments can generate large magnetic reflections. In a polycrystalline sample, magnetic reflections of field-induced magnetic moments are roughly 4π times larger than those of ordered magnetic moments in a long-range order. Here, the factor 4π is the surface area of the unit sphere originating in the random direction of powder. For example, when the detection limit of ordered magnetic moments is 0.2 μ_B, that of field-induced magnetic moments is $0.2/\sqrt{4\pi} \sim 0.06$ μ_B. We can evaluate field-induced magnetic moments of many paramagnets except for spin-gap systems having a nonmagnetic ground state. In ordinary diffraction measurements, reflections are smaller in a polycrystalline sample than in a single-crystal one because of the random direction of powder in the former. The direction of field-induced magnetic moments is parallel to the applied magnetic fields and does not depend on the crystal axes. Therefore the intensities of the magnetic reflections generated by the field-induced magnetic moments in a polycrystalline sample are comparable with those in a single crystal. Single crystals are not necessary for our method.

We believe that it is possible to precisely evaluate exchange interactions in paramagnets with multiple exchange interactions and multiple crystallographic magnetic-ion sites by using field-induced magnetic moments in combination with macroscopic physical quantities because we could precisely evaluate the exchange interactions by using information regarding ordered magnetic moments in conjunction with the magnetic-susceptibility and magnetization results in $Cu_2CdB_2O_6$ [8,9]. This idea is applicable to research of several spin systems such as diamond chain [1–5], spin cluster [20], distorted kagome lattice [21], and three-leg ladder [22,23]. Evaluation of field-induced magnetic moments is also useful in research of magnets containing both transition-metal and rare-earth magnetic ions. It is difficult to evaluate the magnetization of transition-metal ions because it is usually much smaller than the magnetization of rare-earth ions. We can directly study the spin system of transition-metal ions because we can separately evaluate field-induced magnetic moments of transition-metal ions. Many multiferroic materials contain both transition-metal and rare-earth magnetic ions [24]. This idea can contribute to studies of multiferroic materials.

IV. CONCLUSION

We carried out neutron-diffraction experiments in magnetic fields on the paramagnetic state of the spin-$\frac{1}{2}$ AFM trimerized $(J_1 - J_2 - J_2)$ chain compound $Cu_3(P_2O_6OD)_2$ with $J_1 = 111$ K and $J_2 = 30$ K. Magnetic reflections with integer indices appeared at 6 T and 1.6 K, and they were attributed to the field-induced magnetic moments. The magnitudes of the field-induced magnetic moments were $M_1 = 0.43(2)\,\mu_B$/Cu and $M_2 = 0.013(10)\,\mu_B$/Cu on two crystallographic Cu^{2+} (Cu1 and Cu2) sites, respectively, at 6 T and 1.6 K. The value of M_2/M_1 was 0.03(2), and it is the same as the ratio of magnetizations of Cu2 and Cu1 sites calculated for the chain with $J_1 = 111$ K and $J_2 = 30$ K. We confirmed that the information regarding the field-induced magnetic moments was consistent with that regarding the calculated magnetizations in the well-understood spin system (spin chain). We believe that it is possible to precisely evaluate exchange interactions in paramagnets with multiple exchange interactions and multiple crystallographic magnetic-ion sites by using field-induced magnetic moments in conjunction with macroscopic physical quantities. Evaluation of field-induced magnetic moments is useful in research of a wide variety of quantum and frustrated magnets without long-range order.

ACKNOWLEDGMENTS

This work was supported by the Japan Society for the Promotion of Science (JSPS) KAKENHI Grant No. 18K03551, a grant for advanced measurement and characterization technologies accelerating materials innovation (PF2050) from the National Institute for Materials Science (NIMS), and JST-Mirai Program Grant No. JPMJMI18A3, Japan. The travel expenses for the neutron-diffraction experiments were partially supported by the General User Program for Neutron Scattering Experiments, Institute for Solid State Physics, the University of Tokyo (Proposals No. 16801 and No. 18804), at JRR-3, Japan Atomic Energy Agency, Tokai, Japan. The experiments were transferred from 5G:PONTA at JRR-3. We are grateful to Takashi Mochiku, Hiroaki Mamiya, Masamichi Nishino, and Noriki Terada at NIMS for fruitful discussions and to Seiko Matsumoto at NIMS for the sample syntheses and x-ray diffraction measurements.

[1] H. Kikuchi, Y. Fujii, M. Chiba, S. Mitsudo, T. Idehara, T. Tonegawa, K. Okamoto, T. Sakai, T. Kuwai, and H. Ohta, Experimental Observation of the $\frac{1}{3}$ Magnetization Plateau in the Diamond-Chain Compound $Cu_3(CO_3)_2(OH)_2$, Phys. Rev. Lett. **94**, 227201 (2005).

[2] B. Gu and G. Su, Comment on "Experimental Observation of the $\frac{1}{3}$ Magnetization Plateau in the Diamond-Chain Compound $Cu_3(CO_3)_2(OH)_2$),"Phys. Rev. Lett. **97**, 089701 (2006).

[3] H. Kikuchi, Y. Fujii, M. Chiba, S. Mitsudo, T. Idehara, T. Tonegawa, K. Okamoto, T. Sakai, T. Kuwai, and H. Ohta, Experimental Observation of the $\frac{1}{3}$ Magnetization Plateau in the Diamond-Chain Compound $Cu_3(CO_3)_2(OH)_2$–Reply, Phys. Rev. Lett. **97**, 089702 (2006).

[4] J. Kang, C. Lee, R. K. Kremer, and M.-H. Whangbo, Consequences of the intrachain dimer-monomer spin frustration and the interchain dimer-monomer spin exchange in the diamond-chain compound azurite $Cu_3(CO_3)_2(OH)_2$, J. Phys.: Condens. Matter **21**, 392201 (2009).

[5] H. Jeschke, I. Opahle, H. Kandpal, R. Valentí, H. Das, T. Saha-Dasgupta, O. Janson, H. Rosner, A. Brühl, B. Wolf, M. Lang, J. Richter, S. Hu, X. Wang, R. Peters, T. Pruschke, and A. Honecker, Multistep Approach to Microscopic Models for Frustrated Quantum Magnets: The Case of the Natural Mineral Azurite, Phys. Rev. Lett. **106**, 217201 (2011).

[6] T. Masuda, A. Zheludev, B. Grenier, S. Imai, K. Uchinokura, E. Ressouche, and S. Park, Cooperative Ordering of Gapped and

Gapless Spin Networks in $Cu_2Fe_2Ge_4O_{13}$, Phys. Rev. Lett. **93**, 077202 (2004).

[7] M. Matsumoto, H. Kuroe, T. Sekine, and T. Masuda, Transverse and longitudinal excitation modes in interacting multispin systems, J. Phys. Soc. Jpn. **79**, 084703 (2010).

[8] M. Hase, A. Dönni, V. Yu. Pomjakushin, L. Keller, F. Gozzo, A. Cervellino, and M. Kohno, Magnetic structure of $Cu_2CdB_2O_6$ exhibiting a quantum-mechanical magnetization plateau and classical antiferromagnetic long-range order, Phys. Rev. B **80**, 104405 (2009).

[9] M. Hase, M. Kohno, H. Kitazawa, O. Suzuki, K. Ozawa, G. Kido, M. Imai, and X. Hu, Coexistence of a nearly spin-singlet state and antiferromagnetic long-range order in quantum spin system $Cu_2CdB_2O_6$, Phys. Rev. B **72**, 172412 (2005).

[10] M. Hase, M. Kohno, H. Kitazawa, N. Tsujii, O. Suzuki, K. Ozawa, G. Kido, M. Imai, and X. Hu, $\frac{1}{3}$ magnetization plateau observed in the spin-1/2 trimer chain compound $Cu_3(P_2O_6OH)_2$, Phys. Rev. B **73**, 104419 (2006).

[11] M. Hase, M. Matsuda, K. Kakurai, K. Ozawa, H. Kitazawa, N. Tsujii, A. Dönni, M. Kohno, and X. Hu, Direct observation of the energy gap generating the $\frac{1}{3}$ magnetization plateau in the spin-1/2 trimer chain compound $Cu_3(P_2O_6OD)_2$ by inelastic neutron scattering measurements, Phys. Rev. B **76**, 064431 (2007).

[12] R. Baies, V. Caignaert, V. Pralong, and B. Raveau, Copper hydroxydiphosphate with a one-dimensional arrangement of copper polyhedra: $Cu_3[P_2O_6OH]_2$, Inorg. Chem. **44**, 2376 (2005).

[13] S. Paschen, S. Laumann, A. Prokofiev, A. M. Strydom, P. P. Deen, J. R. Stewart, K. Neumaier, A. Goukassov, and J.-M. Mignot, First neutron measurements on $Ce_3Pd_{20}Si_6$, Physica B **403**, 1306 (2008).

[14] M. Hase, T. Yang, R. Cong, J. Lin, A. Matsuo, K. Kindo, K. Ozawa, and H. Kitazawa, High-field magnetization of $SrMn_3P_4O_{14}$ exhibiting a quantum-mechanical magnetization plateau and classical magnetic long-range order, Phys. Rev. B **80**, 054402 (2009).

[15] M. Hase, V. Yu. Pomjakushin, A. Dönni, T. Yang, R. Cong, and J. Lin, Direct observation of the ground state of a $\frac{1}{3}$ quantum magnetization plateau in $SrMn_3P_4O_{14}$ using neutron diffraction measurements, J. Phys. Soc. Jpn. **83**, 104701 (2014).

[16] P. Fischer, G. Frey, M. Koch, M. Koennecke, V. Pomjakushin, J. Schefer, R. Thut, N. Schlumpf, R. Buerge, U. Greuter, S. Bondt, and E. Berruyer, High-resolution powder diffractometer HRPT for thermal neutrons at SINQ, Physica B **276**, 146 (2000); http://sinq.web.psi.ch/hrpt.

[17] J. Rodriguez-Carvajal, Recent advances in magnetic structure determination by neutron powder diffraction, Physica B **192**, 55 (1993); http://www.ill.eu/sites/fullprof/.

[18] O. F. Syljuåsen and A. W. Sandvik, Quantum Monte Carlo with directed loops, Phys. Rev. E **66**, 046701 (2002).

[19] S. W. Lovesey, *Theory of Neutron Scattering from Condensed Matter* (Oxford University Press, Oxford, 1984), Vol. 2.

[20] B. Koteswararao, P. Khuntia, R. Kumar, A. V. Mahajan, A. Yogi, M. Baenitz, Y. Skourski, and F. C. Chou, Bose-Einstein condensation of triplons in the $S = 1$ tetramer antiferromagnet $K_2Ni_2(MoO_4)_3$: A compound close to a quantum critical point, Phys. Rev. B **95**, 180407 (2017).

[21] K. Matan, T. Ono, Y. Fukumoto, T. J. Sato, J. Yamaura, M. Yano, K. Morita, and H. Tanaka, Pinwheel valence-bond solid and triplet excitations in the two-dimensional deformed kagome lattice, Nat. Phys. **6**, 865 (2010).

[22] S. Vilminot, M. Richard-Plouet, G. André, D. Swierczynski, M. Guillot, F. Bourée-Vigneron, and M. Drillon, Magnetic structure and properties of $Cu_3(OH)_4SO_4$ made of triple chains of spins $s = \frac{1}{2}$, J. Solid State Chem. **170**, 255 (2003).

[23] S. Vilminot, G. André, F. Bourée-Vigneron, M. Richard-Plouet, and M. Kurmoo, Magnetic properties and magnetic structures of $Cu_3(OD)_4XO_4$, X = Se or S: Cycloidal versus collinear antiferromagnetic structure, Inorg. Chem. **46**, 10079 (2007).

[24] W. Eerenstein, N. D. Mathur, and J. F. Scott, Multiferroic and magnetoelectric materials, Nature (London) **442**, 759 (2006).